

Time-domain spectroscopy of molecular free-induction decay in the infrared

Ian Coddington,^{1,2} William C. Swann,¹ and Nathan R. Newbury^{1,3}

¹National Institute of Standards and Technology, 325 Broadway, Boulder, Colorado 80305, USA

²ian@boulder.nist.gov

³nnewbury@boulder.nist.gov

Received November 23, 2009; revised February 18, 2010; accepted March 2, 2010;
posted March 25, 2010 (Doc. ID 120276); published April 26, 2010

Time-domain spectroscopy using dual, coherent frequency combs is used to measure free-induction decay from a molecular gas sample in the near-IR with a time-domain signal-to-noise ratio of $\sim 10^6$ over a ~ 6 ns window at 55 fs time resolution (corresponding to the 9 THz source bandwidth) and a frequency/timing accuracy set by the frequency combs. The free-induction decay exhibits the expected periodic pulses from the rephasing of the multiply excited rovibrational levels. This demonstration represents the first high-resolution, high-accuracy, broadband measurement of optical free-induction decay, to our knowledge.

OCIS codes: 320.7100, 140.4050, 120.6200.

A short light pulse will excite resonant molecular transitions in a sample that then act as oscillating dipoles. After the initial excitation, these dipole elements will continue to oscillate coherently, giving rise to coherent forward-scattered radiation or free-induction decay (FID), which can be thought of as the impulse response function of a molecular gas. The forward-scattered field is in exactly the spatial mode of the incident pulse, and the overlap with the incident field yields the standard intensity absorption spectrum observed in optical spectroscopy. As has been widely demonstrated in microwave and terahertz (THz) spectroscopy [1–4], in time-resolved spectroscopy the full FID can be observed. In the optical region of the spectrum, it is challenging to detect FID directly, because of the high carrier frequency. Nevertheless, optical FID has indeed been observed in several experiments [5–8]. In recent work, we demonstrated a dual-comb spectroscopy system that measured the frequency-domain amplitude and phase response of a sample. Here, we emphasize the corresponding time-domain FID signal. (The two are related through a Fourier transform). We discuss significant improvements, including real-time coherent averaging, concurrent normalization through a time-multiplexed reference signal, and automated data acquisition, all made possible by the time-domain character of the signal. Together these advances allow for a near 100% experiment duty cycle and an $\sim 10\times$ improved signal-to-noise ratio (SNR) over [9] with a shorter acquisition period, and the lowest spectral noise floor yet demonstrated with this technique.

The use of dual frequency combs for spectroscopy is expanding rapidly because of their high-frequency accuracy, coherence, and broadband output [9–14]. In dual-comb spectroscopy, asynchronous frequency combs are used to down-mix optical comb light into the rf domain for massively parallel multiheterodyne detection between pairs of comb teeth [9–17]. Viewed as a form of Fourier spectroscopy, this technique has significant overlap with standard Fourier transform IR spectroscopy [18]; however it also differs in sev-

eral ways. First, the use of lasers allows for long interaction paths. Second, in the configuration where only one comb passes through the sample, the interferogram is one sided, as in dispersive FTS, rather than the typical double-sided Fourier transform infrared interferogram. This one-sided interferogram reflects the causality of the signal and results in a frequency-domain signal with both the phase and the amplitude information. Third, the resolution is set by the comb repetition rates (even finer if the combs are scanned) rather than a physical delay line. Fourth, the fractional frequency/timing accuracy is limited only by the underlying frequency comb reference and can easily exceed 10^{-12} . Finally, the signal and reference light can be multiplexed in the time domain, which significantly reduces systematic effects as discussed below.

A simplified schematic of the setup is shown in Fig. 1 [9,16,17]. The two comb sources are stabilized erbium-doped femtosecond fiber lasers with repetition rates $f_r \sim 100$ MHz that differ by $\Delta f_r = 3.14$ kHz. With modest spectral broadening the combs cover an ~ 9 THz bandwidth centered at 1560 nm. Pulses from one comb excite the molecules, and the resulting transmitted signal is a train of unperturbed pulses, each followed by a much longer and weaker tail containing the FID signal. The asynchronous local oscillator (LO) pulse train acts to sample or down-mix both the FID signal and a reference pulse that bypassed the sample. Deconvolution of the reference and signal yields the normalized sample response with an effective frequency resolution limited through apodization to about twice f_r . The nearly continuous measurement of the signal and reference allows for calibration of every interferogram, offering a high degree of immunity to drifts in the laser spectrum or other experimental parameters. Furthermore, with this time-multiplexed approach to normalization, both signal and reference share much of the same optical path and use a common detector, which suppresses ripple in phase or magnitude caused by inadvertent etalon reflections in the optical paths by >30 dB.

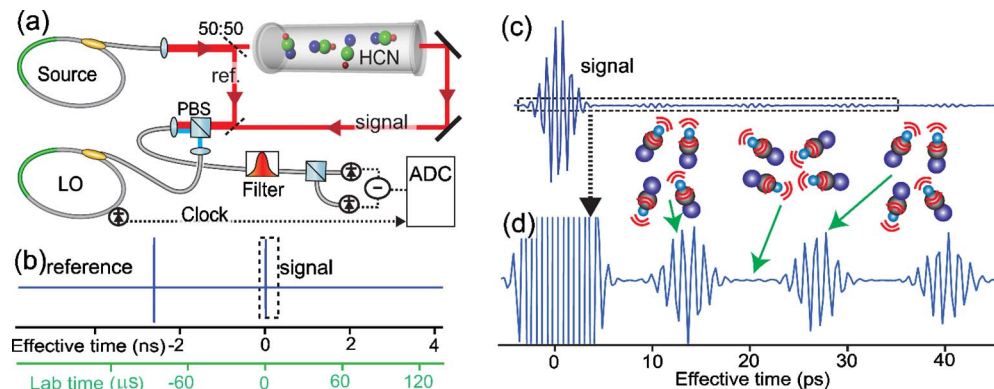


Fig. 1. (Color online) (a) Experimental setup showing lasers, interrogation path, and detection. Half the source pulse train passes through a gas cell of $\text{H}^{13}\text{C}^{14}\text{N}$ gas and half circumvents it to create a reference pulse. The reference and signal pulses are combined with the LO pulse on a polarizing beam splitter (PBS), filtered by a scanning 2 nm bandpass optical filter and detected on a balanced detector. (b) Example data showing the measured reference and signal pulses, in effective time (i.e., the time delay between signal and LO pulses), after 100,000 averages (30 s) for a filter centered at 195 THz and a 15 cm, 25 Torr cell. (c) Expanded view of the signal pulse [box in part (b)]. (d) Further expanded view. The signal consists of the incident pulse followed by the trailing FID signal, which exhibits ringing as the ensemble of vibrating rotating molecules periodically realign to radiate coherently in the forward direction.

While it would be possible to detect the entire 9 THz spectrum at once, the peak signal would exceed the dynamic range of the commercial balanced detector and 12 bit digitizer; therefore we use a tunable optical filter (coarse spectrometer) with 2 nm (250 GHz) bandwidth. (This also limits the instantaneous signal bandwidth to below the effective Nyquist limit set by our choice of f_r and Δf_r [9–17].) The response is acquired as the filter is stepped across the spectrum, and finally the total signal is coherently stitched together over the full 9 THz from the baseline-corrected response at each setting. The LO comb is frequency shifted for filter settings that would otherwise yield a heterodyne signal at baseband or Nyquist. An inverse Fourier transform yields the full FID signal. In addition to mitigating the dynamic range limit, the use of a tuned filter flattens the optical spectrum and puts stringent limits on aliasing.

The LO pulse train scans or walks through the entire signal pulse period every $\Delta f_r^{-1} \sim 320 \mu\text{s}$ to generate a single interferogram. Because of the dynamic range limitations of the detection, the SNR on one interferogram is poor and is improved through coherent signal averaging without excessive data storage by phase locking the two comb sources such that the LO and signal pulses always arrive at the beginning of each 320 μs interferogram with exactly the same pulse and carrier overlap [17]. Under these conditions, we simply add successive interferograms (and FID signals) either in firmware or software for up to ~ 3 s, limited by drifts in the relative optical paths. For averaging times beyond 3 s, averaged interferograms are phase corrected based on the centerburst [19] before co-adding [see Fig. 1(b)].

Figure 2(a) shows the measured FID decay from the C—H overtone stretch vibration in hydrogen cyanide (HCN). In effective time, the trace extends from ~ 2 ns before the incident pulse to ~ 4 ns after the pulse at a time resolution of 55 fs, yielding 110,000 data points. The noise background is the

same before and after the pulse (as verified with an empty cell), and the SNR is 0.5×10^6 . The corresponding frequency-domain noise varies but is $\sim 2.5 \times 10^{-4}$ in both phase (radians) and amplitude near the center [see Fig. 2(d)], with an additional small 5×10^{-4} ripple due to residual comb phase noise. Because of downsampling and the coherent signal averaging, these low SNR levels are reached at an effective scan rate of 200 GHz/min in real time or 2700 s for the full 9 THz. The SNR scales as the square root of acquisition time, and much shorter acquisition times are easily realized with a corresponding loss of SNR.

The FID time-domain response is simply related to the complex linear susceptibility, $\chi(\nu)$, as the Fourier transform of $[1 + i4\pi^2 c^{-1} \nu L \chi(\nu)]$ over the 9 THz window, where L is the cell length. For a set of rovibrational lines at frequencies ν_i , line strength S_i , Doppler FWHM $\Delta\nu_D$, and collisional FWHM $\Delta\nu_{Li}$, the time-domain response is $1 - \rho L \Delta t \sum_i 2S_i \cos(2\pi\nu_i t) \theta(t) e^{-\pi^2 \Delta\nu_D^2 t^2 / (4 \ln 2) - \pi \Delta\nu_{Li} t}$, where ρ is the number density, $\theta(t)$ is the Heaviside step function, and Δt the time resolution ($= 55$ fs). See Fig. 2(b) for a comparison of the data with this equation.

Because of the number of rotational levels, the FID structure is complicated, and it is convenient to use a sonogram to spread the information out over time and frequency as shown in Fig. 2(c). In this sonogram the vertical strip at $t=0$ is the incident signal pulse, and the trailing slowed light signal at later times is the FID. Because the rotation speeds are quantized, the molecules periodically rephase to generate additional pulses of coherently forward-scattered light called commensurate echoes [3]. These echoes are visible as vertical striations in the data and can yield information on molecular constants. For the P branch (lower frequency) and the R branch the recurrences occur with a period of $(2B'' - 2(B' - B''))J^{-1} = 10.5$ ps and $(4B' - 2B'' + 2(B' - B''))J^{-1} = 13.4$ ps, re-

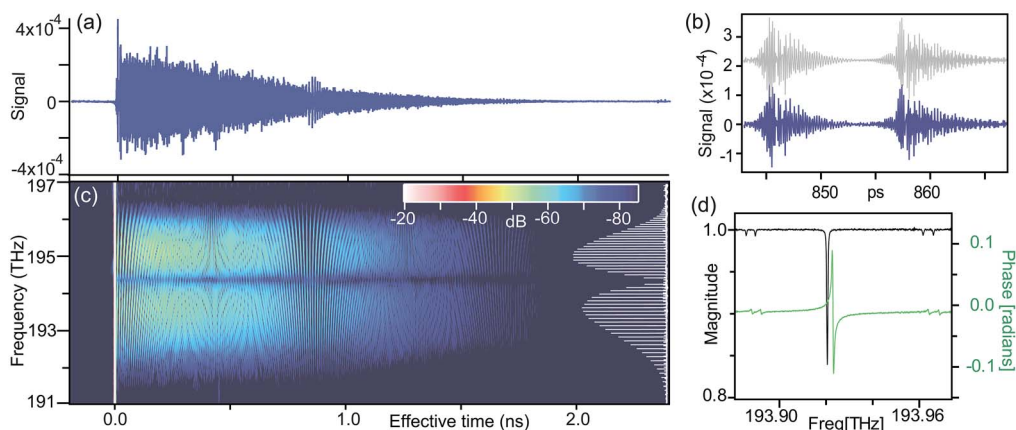


Fig. 2. (Color online) Reconstructed FID for a 2.7 Torr, 20 cm $\text{H}^{13}\text{C}^{14}\text{N}$ cell. (a) The FID with the peak at $t=0$ normalized to one (off scale). (b) Expanded view of the FID from (a) compared with a simulation (gray, offset line). (c) Sonogram (i.e., short-time Fourier transform) of the FID with 200 GHz and 5 ps resolution (false color, log scale). The pulse peak is normalized to 0 dB. On the right is the HCN absorption spectrum to guide the eye. (d) The corresponding frequency-domain response magnitude (black) and phase (green, offset for clarity) of a single molecular line, demonstrating the high SNR and flat baseline. Small peaks to either side are hot bands.

spectively, where B'' (B') is the ground (excited) state rotational constant, and we assume an average J value of 8 [19]. Depending on the spectral region, 140–170 rotational recurrences are visible out beyond 1.8 ns. Because of the J dependence of rotational frequencies the recurrences slowly dephase, with broadband realigning again at intervals of $[2(B' - B'')]^{-1} = 0.853$ ns for both branches.

While the SNR is significantly improved over [9], higher SNR is always desirable. The noise is roughly 80% detector noise and 20% shot noise; however, the real limit is set by the detector dynamic range. Employing the tunable filter to break up the spectrum reduces the peak signal and improves the overall SNR roughly as the square root of the number of filter positions. This dynamic range also could be increased through an improved detector, applying a differential chirp between the combs [11,13,18] or ignoring the saturating centerburst [2]. An even larger SNR increase would result from parallel acquisition incorporating multiple narrowband filters and a detector array [20].

The true promise of this approach clearly lies in achieving higher SNR and in moving to the mid-infrared [10,11], where molecular cross sections are larger. Finally, it is intriguing to consider combining such a comb system with synchronous pump–probe spectroscopy or nonlinear spectroscopic techniques such as 2D Fourier transform spectroscopy.

We acknowledge useful discussions with A. Bartels, S. Diddams, E. Grossman, and A. Zolot.

References

1. A. Abragam, *The Principles of Nuclear Magnetism* (Clarendon, 1961).
2. B. C. Dian, G. G. Brown, K. O. Douglass, and B. H. Pate, *Science* **320**, 924 (2008).
3. H. Harde, S. Keiding, and D. Grischkowsky, *Phys. Rev. Lett.* **66**, 1834 (1991).
4. A. Bartels, R. Cerna, C. Kistner, A. Thoma, F. Hudert, C. Janke, and T. Dekorsy, *Rev. Sci. Instrum.* **78**, 035107 (2007).
5. R. G. Brewer and R. Shoemaker, *Phys. Rev. Lett.* **27**, 631 (1971).
6. A. Z. Genack, D. A. Weitz, R. M. Macfarlane, R. M. Shelby, and A. Schenzle, *Phys. Rev. Lett.* **45**, 438 (1980).
7. T. Mishina and Y. Masumoto, *Phys. Rev. Lett.* **71**, 2785 (1993).
8. N. Tsurumachi, T. Fuji, S. Kawato, T. Hattori, and H. Nakatsuka, *Opt. Lett.* **19**, 1867 (1994).
9. I. Coddington, W. C. Swann, and N. R. Newbury, *Phys. Rev. Lett.* **100**, 013902 (2008).
10. F. Keilmann, C. Gohle, and R. Holzwarth, *Opt. Lett.* **29**, 1542 (2004).
11. A. Schliesser, M. Brehm, F. Keilmann, and D. van der Weide, *Opt. Express* **13**, 9029 (2005).
12. T. Yasui, Y. Kabetani, E. Saneyoshi, S. Yokoyama, and T. Araki, *Appl. Phys. Lett.* **88**, 241104 (2006).
13. P. Giaccari, J. D. Deschenes, P. Saucier, J. Genest, and P. Tremblay, *Opt. Express* **16**, 4347 (2008).
14. B. Bernhardt, A. Ozawa, P. Jacquet, M. Jacquy, Y. Kobayashi, T. Udem, R. Holzwarth, G. Guelachvili, T. W. Hansch, and N. Picque, *Nat. Photonics* **4**, 55 (2009).
15. S. Schiller, *Opt. Lett.* **27**, 766 (2002).
16. I. Coddington, W. C. Swann, L. Nenadovic, and N. R. Newbury, *Nat. Photonics* **3**, 351 (2009).
17. I. Coddington, W. C. Swann, and N. R. Newbury, *Opt. Lett.* **34**, 2153 (2009).
18. P. R. Griffiths and J. A. Haseth, *Fourier Transform Infrared Spectrometry* (Wiley-Interscience, 2007).
19. W. C. Swann and S. L. Gilbert, *J. Opt. Soc. Am. B* **22**, 1749 (2005).
20. N. R. Newbury, I. Coddington, and W. C. Swann, *Opt. Express* **18**, 7929 (2010).